Biophysical Chemistry 167 (2012) 8–15

Contents lists available at SciVerse ScienceDirect

Biophysical Chemistry

journal homepage: http://www.elsevier.com/locate/biophyschem

L27–tRNA interaction revealed by mutagenesis and pH titration

Ming Xiao, Yuhong Wang *

Department of Biology and Biochemistry, University of Houston, 4800 Calhoun Rd, Houston, TX 77214, USA

HIGHLIGHTS

► Truncation of the ribosomal protein L27 N-terminal residues increases peptidyl tRNA fluctuation.
► Elevation of the solution pH increases peptidyl tRNA fluctuation.
► The K4 residue H-bonds with the "P-loop" via the "induced-fit" after substrate binding.

GRAPHICAL ABSTRACT

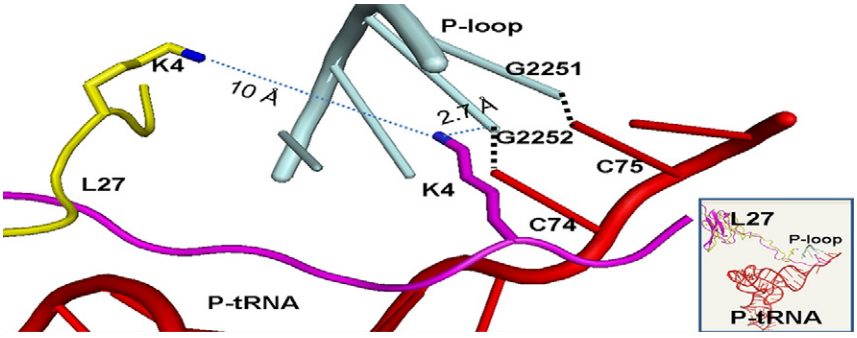

ARTICLE INFO

Article history:
Received 20 March 2012
Received in revised form 23 April 2012
Accepted 27 April 2012
Available online 7 May 2012

Keywords:
Single-molecule FRET
pH titration
Ribosome fluctuation
Ribosome translocation
Ribosome "unlock"
Peptidyl transfer center

ABSTRACT

The movement of peptidyl tRNA into the P-site after ribosome translocation reduces the ribosome dynamics in the post-translocation complex, which "locks" the ribosome to less conformational fluctuations. Here, we used single molecule FRET method to reveal that ribosomes bearing L27 with N-terminal truncations are less competent to "lock" the tRNA fluctuations after translocation. We found that: (1) truncation of the first three N-terminal residues of L27 increases peptidyl tRNA fluctuation; and (2) increasing the solution pH increases peptidyl tRNA fluctuation in WT and some of the ribosome mutants. We propose that one role of L27 at the catalytic center is to stabilize peptidyl tRNA in the post-translocation complex.

1. Introduction

The ribosome is a 2.6 MDa molecular device consisting of 3 rRNA chains and 50–80 proteins. The ribosome small subunit (30S) recruits the mRNA template for protein translation, while the large subunit (50S) accommodates the tRNA substrates and the elongating peptidyl chain. There are three tRNA binding sites (A, P and E) in both the 30S and the 50S subunits. Therefore, the tRNA configuration is expressed in two letters, such as "A/A". The first and the second letters refer to the tRNA-binding site in the small and the large subunits, respectively. The new amino acid is conveyed into the 50S A-site by the aminoacyl-tRNA, followed by a peptidyl transfer reaction to elongate the peptidyl chain. The ribosome is then at the pre-translocation stage. In this ribosome complex, the tRNA configurations are: A/A-bound peptidyl tRNA and P/P-bound deacylated tRNA (A/A–P/P). During the following translocation process, the ribosome translocase EF-G ensures the correct movement of the mRNA and the tRNAs. The ribosome is then at the post-translocation stage. In this ribosome complex, the tRNA configurations are: P/P-bound peptidyl tRNA and E/E-bound deacylated tRNA.

The ribosome alternates its dynamics at the pre- and post-translocation stages. In the pre-translocation complex, the ribosome

* Corresponding author at: 4800 Calhoun Rd, University of Houston, Houston, TX 77204, USA. Tel.: +1 713 743 7941; fax: +1 713 743 8651.
E-mail address: ywang60@uh.edu (Y. Wang).

0301-4622/$ – see front matter © 2012 Elsevier B.V. All rights reserved.
doi:10.1016/j.bpc.2012.04.003

undergoes inter-subunit ratcheting [1] and the tRNAs undergo classical-hybrid state fluctuations ("A/A–P/P" "A/P–P/E") [2]. The "A/P–P/E" represents a tRNA hybrid configuration in which the tRNAs are bound at the A- and P-sites in the 30S but at the P- and E-sites in the 50S. In the post-translocation complex, the peptidyl-tRNA moves into the P-site to "lock" the ribosome fluctuation, diminishing the conformational flexibility. The ribosome is mostly in the un-ratcheted state, and tRNAs remain in the classical state ("P/P–E/E"). Whether tRNA and ribosome dynamics are tightly coupled is under debate [3–5], but it is clear that the un-ratcheted ribosome favors the classical bound tRNAs and that the ratcheted ribosome is essential to form hybrid tRNAs and for ribosome fluctuations [3,6,7]. The alternative ribosome "unlocking" and "locking" were first reported by fast kinetics [8] and Cryo-EM [9], and later supported by other studies [10–14]. The key component to trigger the alternative ribosome dynamics is the peptidyl tRNA. When the peptidyl tRNA is at the P-site, the ribosome is locked into the classical state, whereas when the peptidyl tRNA is at the A-site, the ribosome is unlocked and is able to sample the ratcheted state [9]. However, the mechanisms to trigger these changes are not known.

The location of the N-terminus of ribosomal protein L27 within H-bond distance to both the A- and P-site tRNAs suggests its possible role in monitoring the peptidyl tRNA. Indeed, structural studies have shown that residues A2 and H3 together with G6, L7 and R11, interact with the A- and P-site tRNAs [15]. These interactions explained the photo-crosslinking experiments, which showed that the first three N-terminal residues were within 2–3 Å of the P-site tRNA [16].

In this report, we have studied the peptidyl-tRNA dynamics in the "locked" post-translocation complex via single-molecule fluorescence resonance energy transfer (FRET) measurements. Removal of the first two N-terminal amino acids of L27 in the ribosome (Rb-AH) does not cause significant changes to the stability of the P-site-bound tRNA, as deduced from its FRET signal with the L27 protein. The first and second residues of L27 are A2 and H3 because the universal fMet is removed in situ in mature L27 [16–18]. However, removal of the first three amino acids in Rb-AHK significantly reduces the stability of the P-site-bound tRNA. In addition, increasing the pH causes tRNA instability in Rb-WT and Rb-AH but does not exert an apparent effect on Rb-AHK. Our results suggest that the residue K4 either directly or indirectly interacts with the peptidyl tRNA and causes the observed pH responds. Based on sequences information from NCBI (National Center for Biotechnology Information), the A2, H3, and K4 residues are approximately 60–70% conserved in bacterial. The N-terminal sequence of "AHKK" is 100% conserved in some species, including *Escherichia coli*, *Mycobacterium tuberculosis*, *Vibrio cholerae*, *Thermus* thermophiles, etc.

2. Results and discussion

2.1. Characterization of L27 reconstituted ribosomes

We have prepared three types of L27: L27-WT, L27-AH in which the first two residues A2H3 were removed, and L27-AHK in which the first three residues A2H3K4 were removed. The L27 truncations were directly confirmed by their N-terminal sequences. These proteins were labeled with the Cy5 dye (receptor) and then incorporated into the ribosomes from *E. coli* strain IW312 lacking the protein L27 [19]. The ribosomes incorporated with the three L27s are termed as Rb-WT, Rb-AH, and Rb-AHK, respectively. The protein incorporation efficiency was estimated from the ratio of ribosome absorbance at 260 nm and the Cy5-labeled protein absorbance at 650 nm. The L27 incorporated into the IW312 ribosome with 100% efficiency, while its nonspecific binding to the WT ribosome (MRE 600) was approximately 10–20% efficient.

The correct incorporation of the L27 to its designated position inside the ribosome was confirmed by the regained ribosome activity in polyphenylalanine synthesis (poly(Phe) assay). In this assay, the ribosome was charged with poly(U) synthetic mRNA and the ribosome activity was measured by the amount of ^{14}C-labeled poly(Phe) generated at: 0.5, 1, 5 and 30 min. As shown in Fig. 1, the poly(Phe)-synthesizing activity of the normal ribosome strain MRE600 was used as the reference. Compared to this reference, the L27-lacking ribosome strain IW312 had low activity. The incorporations of the WT or mutated L27 proteins L27-AH and L27-AHK into the IW312 ribosomes revived them to full activity compared with the reference.

The correct incorporation of L27 into the IW312 ribosome was also confirmed by single-molecule FRET measurement. The complexes prepared from the IW312 ribosomes incubated with Cy5-labeled L27 generated at least three biologically active FRET states, as we have reported [3,11,17]. However, the complexes prepared from the MRE600 ribosome incubated with Cy5-labeled L27 generated zero FRET signals. Given the large size of the ribosome (20 nm in diameter), it is unlikely that an L27 randomly docked on the ribosome in multiple preparations always FRETs with tRNAs with consistent efficiency. Therefore, our FRET measurement itself demonstrates that the L27 was at the correct location inside the ribosome.

2.2. 70–80% completeness of the translocation process

The completeness of the post-translocation process in our single-molecule experiments was estimated by the puromycin assay "SPARK" [20]. In this assay, the ribosome complex is tethered to the streptavidin coated SPA beads, which can only detect radioactivity on its surface. The antibiotic puromycin binds at the empty A-site and attacks the radioactively labeled peptidyl chain to cause the nascent polypeptide to drop off. The percentage of the drop-off is detected by the radioactivity decrease because only ribosome-bound peptides give radioactive signals (Experimental section). The puromycin reaction is more than several-thousand-fold faster in the post- than in the pre-translocation complex because of the availability of the A-site binding pocket for the antibiotic [21,22]. Nevertheless, due to the hybrid state formation and spontaneous translocation process, ribosome pre-translocation complexes react with puromycin to a lesser extent. Fig. 2 shows that approximately 20–30% of the pre-translocation complex reacted with puromycin. These results agree well with published values at similar puromycin concentrations [23]. In the post-translocation complex, all types of ribosomes underwent 70–80% puromycin reaction (Fig. 2). These measurements agree well with previous single-molecule FRET measurements [11]. These measurements were based on active ribosomes that have been tethered to the SPA beads via the mRNA–biotin–streptavidin-bead linkage (Experimental section). The inactive ribosomes that did not form the correct complexes were incapable of either binding to the SPA beads or responding to puromycin treatment, therefore were invisible in our experiments.

2.3. Strategy of FRET labeling and subpopulation sorting

As shown in Figure S1, ribosomal protein L27 was labeled with Cy5 dye at the unique residue Cys53 [11], while tRNA^{Phe} was labeled with Cy3 dye at the D-loop [24]. In the pre-translocation complex bearing a vacant tRNA^{fMet} at the P-site and the Cy3-labeled dipeptide-tRNA (Cy3·fMet-Phe-tRNA^{Phe}) at the A-site, the major ribosome subpopulation displayed a Gaussian shaped FRET efficiency distribution centered at 0.47. In the post-translocation complex bearing Cy3·fMet-Phe-tRNA^{Phe} at the P-site and a vacancy at the A-site, the major ribosome subpopulation displayed a Gaussian shaped FRET efficiency distribution centered at 0.68. These FRET values indicate that the distance between the C53 residue on L27 to the P-site tRNA is shorter than the distance between the C53 and the A-site tRNA, which agrees with the X-ray structural study [11]. In addition, for the same pre-translocation complex, changing the dye-labeling position from the A-site-bound tRNA^{Phe} to P-site-bound tRNA^{fMet}

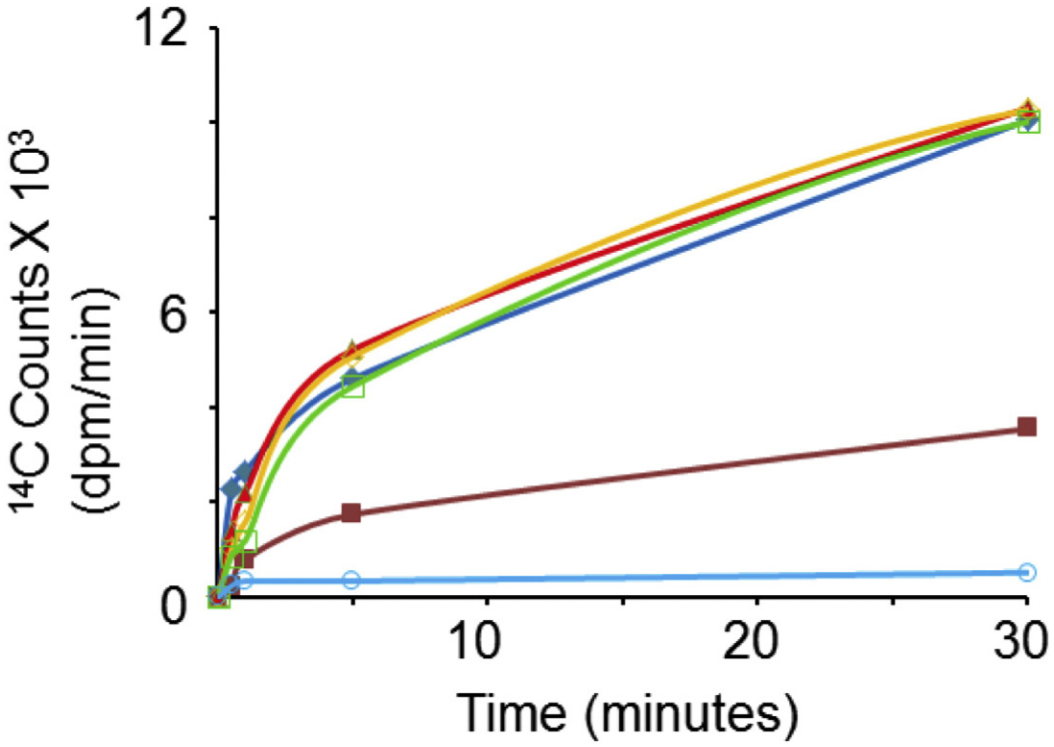

Fig. 1. The poly(Phe) assay to characterize the ribosomes reconstituted in vitro with WT and mutated L27 proteins. The ribosomes are charged with synthetic poly(U) mRNA and the activities are measured by the amount of ^{14}C-labeled Poly(Phe) generated at several time points (0.5, 1, 5 and 30 min). Without L27, the IW312 ribosome has low activity, whereas incorporation of L27 into IW312 restores the activity to a level comparable to that of the MRE 600 ribosome (the wild type ribosome with intact L27 and normal activity). The background control is with the MRE600 ribosome without poly(U). (◆), MRE 600 ribosome; (■), IW312 ribosome; (▲), Rb-WT; (◊), Rb-AH; (⊟), Rb-AHK, (⊖) MRE 600 ribosome with no poly(U).

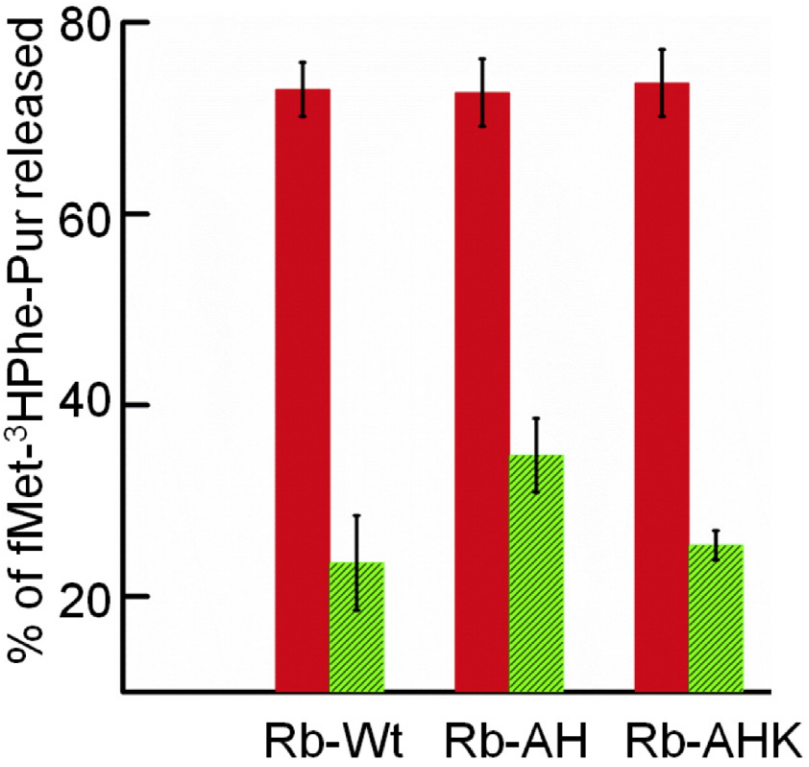

Fig. 2. Puromycin reaction of pre- (bar with pattern) and post-translocation (bar with solid fill) complexes. Puromycin detaches fMet-^{3}H-Phe from the tRNA^{Phe} in ribosomal complexes tethered on SPA beads. The extent of the puromycin reaction is deduced from the differences in radioactivity between ribosomes treated with vs. without puromycin (described in the Experimental section).

shifted the major FRET peak from 0.47 to 0.68 [3]. Importantly, the transition from the 0.47 to the static 0.68 FRET states concurrent with the tRNA translocation process in the presence of the ribosome translocase EF-G was observed in real time [11]. Based on these observations, the 0.47 and 0.68 FRET states were assigned as the A*/A*–P/P and P*/P* configurations for the pre- and post-translocation complexes, respectively (Figure S2). The "*" symbol marked the location of the labeled tRNA.

All of the selected fluorescence traces showed signal-to-noise ratios greater than 4:1 and were bleached at a single step. Traces with multiple bleaching steps were rare and were not included in data analysis. FRET efficiencies were calculated according to the equation $\mathrm{FRET} = I_{\mathrm{acceptor}}/(I_{\mathrm{acceptor}} + I_{\mathrm{donor}})$. The calculated FRET efficiencies were then analyzed by histograms (Fig. 3). The FRET efficiency traces were truncated at several points prior to the bleaching events to remove the artificial FRET signals due to background fluorescence noises or donor crosstalk after acceptor bleaching (Figure S3). Without these truncations, the donor crosstalk produced one additional large FRET peak at approximately 0.045, which could interfere with the Gaussian fitting (Figure S4).

Fig. 3 presents the FRET efficiency histogram analysis of the Rb-WT post-translocation complex at pH 7.4. Because of the 70–80% translocation completeness in vitro, some pre-translocation complex remained in the reaction mixture, which can be filtered out based on the absence of the 0.68 FRET state (110 ribosomes in Fig. 3). Out of the remaining 740 ribosomes, there were 493 non-fluctuating (NF) and 247 fluctuating ribosomes (F). Both of these subpopulations displayed the 0.68 FRET states. The NF ribosomes were defined by Pearson's correlation coefficient between the donor and acceptor fluorescence intensities within ± 0.15. The F ribosomes were defined by the anti-correlative fluctuation between the donor and the acceptor fluorescence intensities (Pearson's correlation coefficient < -0.6). One example from each subpopulation is shown in Fig. 3. The presence of the F ribosome implied that in a minor ribosome subpopulation, the peptidyl tRNA was able to fluctuate. Because the ratcheted ribosome is essential for tRNA fluctuation, the observation of F

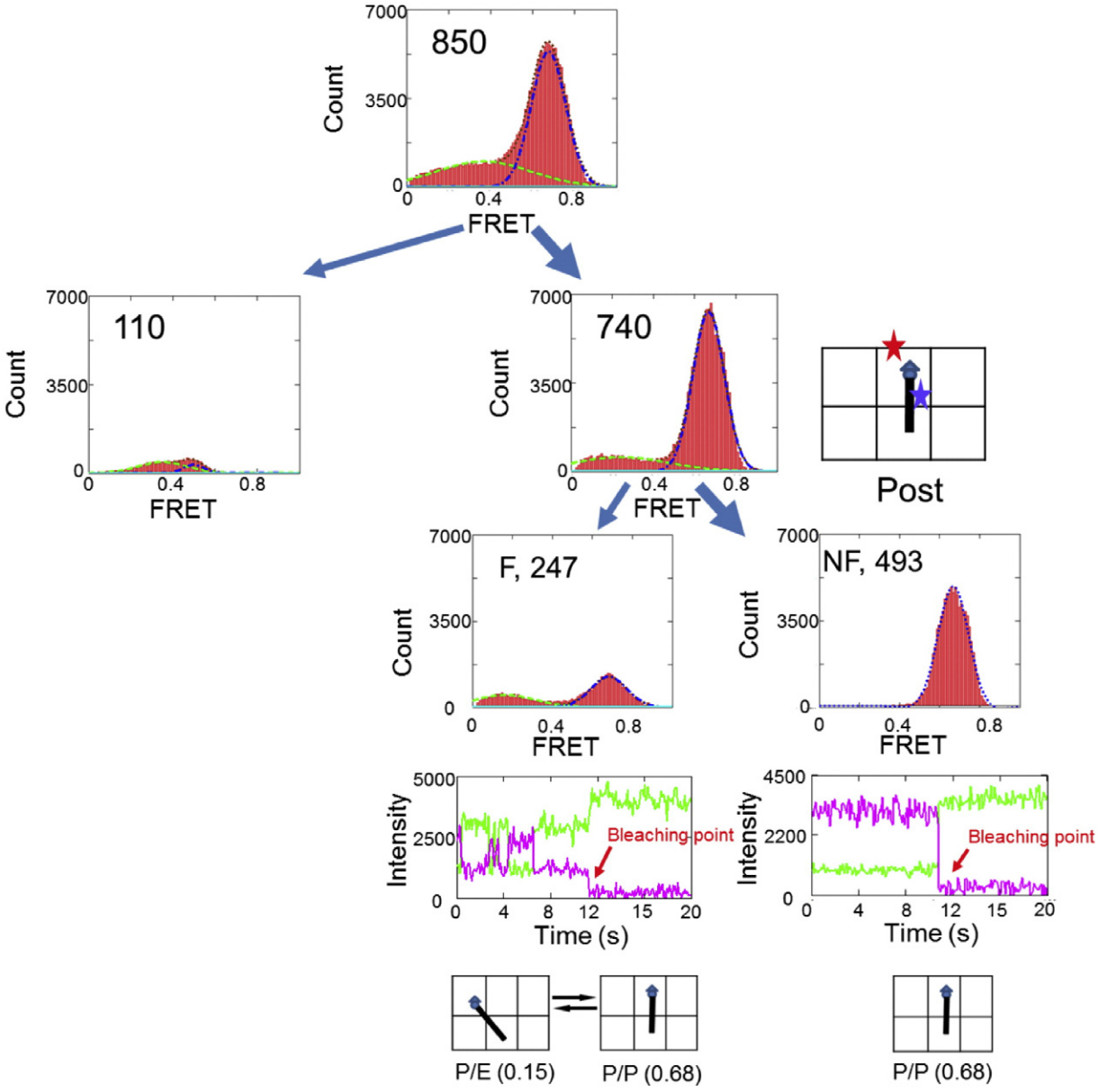

Fig. 3. The FRET efficiency histograms of the F and NF subpopulations in the Rb-WT post-translocation complex at pH 7.4. The second tier shows removal of the pre-translocation ribosomes based on the absence of the 0.68 FRET state. The third tier shows the histogram of the F and NF subpopulations separately. The fourth tier shows one representative pair of donor/acceptor fluorescence intensity traces from each of the subpopulations.

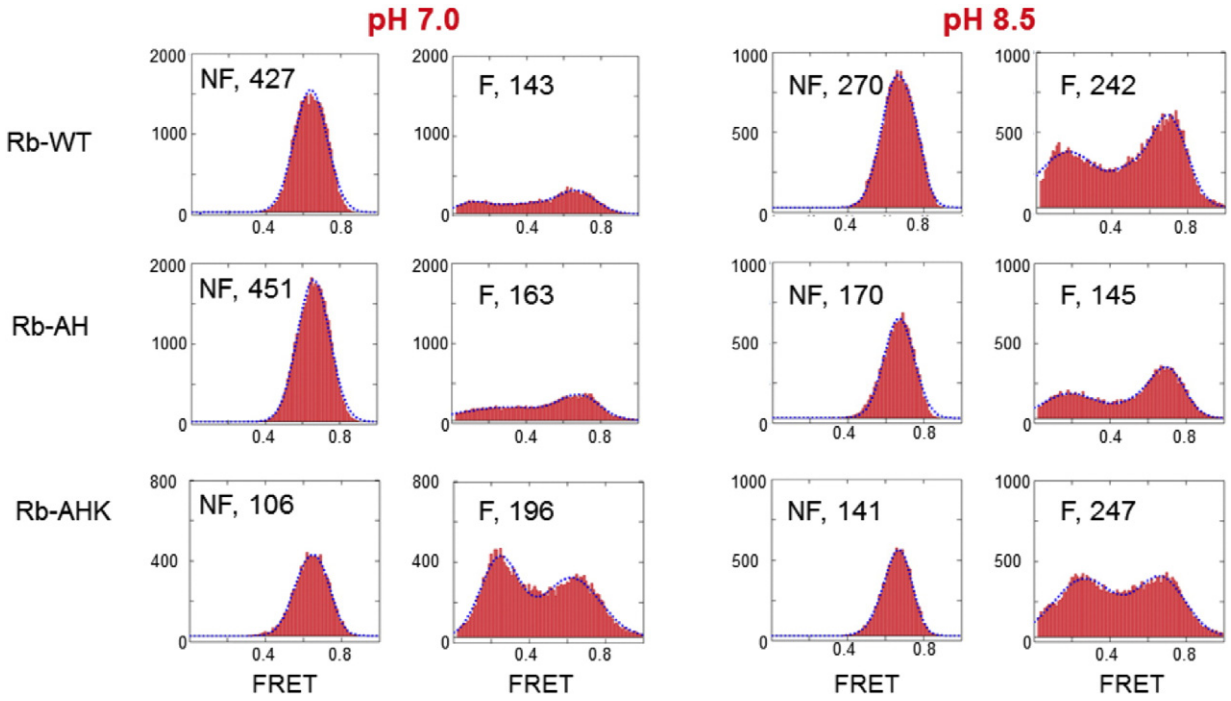

Fig. 4. The FRET efficiency histograms for the F and NF subpopulations in the post-translocation complexes of Rb-WT and the mutants at pH 7.0 and pH 8.0. Either mutating L27 (compared vertically) or elevating the pH (compared horizontally) causes changes in the compositions of the F and NF subpopulations. One set of data for each condition is shown.

subpopulation is in line with a previous single-molecule study showing that "locked" post-translocation complex could nevertheless adapt the ratcheted conformation [10]. We postulate that this fluctuation is due to "P*/P* P*/E*" exchange. Approximately 5–10% of the F subpopulation displayed the exchange from the NF to the F conformation in all ribosome species we studied in the full pH range (Figure S5), which implies that both F and NF subpopulations are valid conformations on the energy landscape of the post-translocation complex.

As we reported before, one subpopulation of the pre-translocation ribosome transiently samples the hybrid state "A*/P*–P/E" [11]. This hybrid state displays a similar FRET efficiency at 0.68, therefore, could not be filtered out from the post-translocation complex signal. Based on previous studies, the amount of this subpopulation can be estimated to be half of the other subpopulations (110 ribosomes in Fig. 3), accounting 1/3 of the total pre-translocation complex. Subtracting this number from the fluctuating subpopulation in the post-translocation complex, we estimated the F population in the post-translocation complex to be 192 ribosomes ($247-55=192$). The percentage of the NF subpopulation in the competent post-translocation complex was calculated to be 72% ($493/(493+192)$). If this pre-translocation subpopulation was not corrected, the apparent NF subpopulation was calculated to be 67% ($493/(493+247)$). The difference does not change the subsequent analysis and conclusions. Nevertheless, all of the composition analyses for the post-translocation complexes in this report were calculated with the corrections.

2.4. Changes of the subpopulation composition with ribosome mutants and at varied pH

The composition of the F and NF subpopulations in the post-translocation complex changed in ribosome mutants and in buffers with different pH values. Fig. 4 displays some examples of the FRET efficiency histograms at pH 7.0 and pH 8.5 from all three ribosome species (one set of data are shown). At each pH, Rb-AHK generated more F ribosomes than Rb-WT and Rb-AH. For Rb-WT and Rb-AH, pH 8.5 induced more F ribosomes than pH 7.0. Rb-AHK did not change its subpopulation composition with pH.

The subpopulation compositions calculated in the form of NF/(NF + F) are displayed in Fig. 5 at seven different pH values in the range of 7.0 to 8.5. The values are obtained after the correction of the residual pre-translocation complex signals from the F-subpopulations, similar to the data in Fig. 3. For each data point, at least three sets of independent measurements are included. Along the *y*-axis and comparing different ribosome species at pH ≤ 8.0, Fig. 5 shows that the elimination of three N-terminal residues from L27 caused a decrease of the NF subpopulation in Rb-AHK compared to Rb-WT. Rb-AH maintained a similar NF composition when compared with Rb-WT, whereas ribosomes bearing L27-AHK underwent a significant decrease in NF/(NF + F) to 50–60%. At pH 8.5, all three species of ribosome converged to generate similar subpopulation compositions (NF/(NF + F) approximately 50–60%).

On the other hand, along the *x*-axis in Fig. 5 and comparing the pH effects on the subpopulation composition in each ribosome species, the NF/(NF + F) ratio decreased in Rb-WT and Rb-AH but did not change in Rb-AHK. For Rb-WT, the NF/(NF + F) ratio decreased gradually from 81 ± 2% at pH 7.0 to 59 ± 2.5% at pH 8.5. A relatively flat region was observed between pH 7.4 and 7.8. For Rb-AH, a similar decreasing trend was observed. However, for Rb-AHK, there was no change in NF/(NF + F) with pH. The subpopulation composition remained at approximately 50–60% between pH 7.0 and pH 8.5.

These observations prompted us to hypothesize that the K4 residue of L27 is probably involved in stabilizing the NF subpopulation and this interaction is sensitive to solution pH values. In Rb-WT and Rb-AH, the percentage of the NF subpopulation decreased with pH elevation. In Rb-AHK, the K4 residue was absent, so the proportion of the NF was lower compared to the other two ribosome species and was not sensitive to pH. At pH 8.5, all three ribosomes had similar NF subpopulation representations.

3. Conclusion

The faithful translation of genes depends on the exact translocation of the mRNA inside the ribosome small subunit (30S) on every three nucleotides. The putative model is that this process occurs in a stepwise manner. In the first step, the tRNAs translocate from the

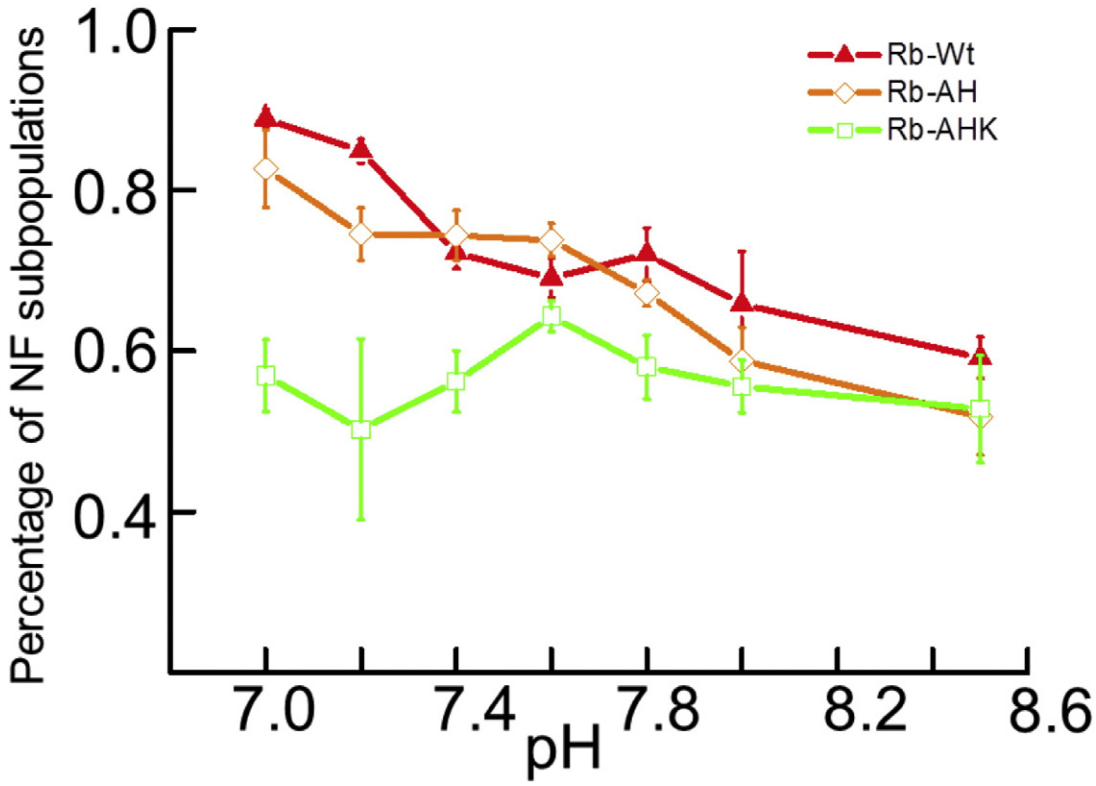

Fig. 5. The pH titration curves for the subpopulation compositions in the post-translocation complexes for Rb-WT (▲), Rb-AH (◊), and Rb-AHK (□). The *x*-axis shows the pH values of 7.0, 7.2, 7.4, 7.6, 7.8, 8.0 and 8.5. The *y*-axis shows the ratio of NF/(NF + F). This ratio is corrected from the contamination of the pre-translocation complex signal as described in the text. In both the horizontal and vertical directions, the NF/(NF + F) ratio decreases which implies that either removal of K4 from L27 or deprotonation of this residue exert similar effects on the ribosome dynamics.

A/A–P/P to the A/P–P/E configuration [2]; meanwhile, the 30S rotates a few degrees relative to the 50S [1]. In the second step, the tRNAs translocate from A/P–P/E to P/P–E/E, while the 30S rotates back from its ratcheted state to its original orientation. During the second step, the mRNA travels three nucleotides inside the 30S subunit [25]. The intermediate state in this process, the hybrid state, is demonstrated to be biologically relevant [21,26]. It has been proposed that the formation of the hybrid state and the subsequent interactions of the ribosome with the correct G-protein factors are regulated by the position of the peptidyl chain [9,23]. Before translocation, the peptidyl chain is attached to the A-site tRNA, and the ribosome forms the hybrid state with fluctuating dynamics (the unlocked state); meanwhile, the ribosome interacts with the factor EF-G favorably for translocation. After translocation, the peptidyl-tRNA moves into the P-site, and the ribosome forms the classical state with static dynamics (the locked state); meanwhile, the ribosome interacts with the factor EF-Tu favorably for another round of tRNA uptake. However, it is not clear what are the specific sensors in the ribosome that detect the location of the peptidyl tRNA to tune the unlocked–locked dynamics of the ribosomes.

Here, we report that L27 stabilizes the peptidyl tRNA. Removal of the three N-terminal residues from this protein in Rb-AHK caused an increase in peptidyl tRNA fluctuation. Increasing the solution pH also caused an increase in tRNA fluctuation in Rb-AH and Rb-WT but did not affect Rb-AHK, which lacked the residue K4 (Figs. 4 and 5). Therefore, L27 stabilizes the peptidyl tRNA and the residue K4 probably causes this interaction to be sensitive to pH values. Given the essential role of the peptidyl tRNA in locking the ribosome dynamics, our data suggests that the L27 protein is possibly another ribosome components that monitor the peptidyl tRNA location, in addition to the well-known interaction between the peptidyl tRNA and the "P-loop" [27].

The structure of the ribosome bearing two complete tRNA substrates shows that the residue K4 of L27 (magenta colored in Fig. 6) forms an H-bond with the O6 of G2252 on the 23S "P-loop". This nucleotide forms a cognate C-G base pair with the C74 of tRNA (Fig. 6). This interaction network can explain the essential role of the K4 residue to maintain the NF-subpopulation in our experiments. However, overlaying the L27 from another ribosome structure [28] bearing no tRNA substrates (yellow colored) shows that this L27–tRNA interaction could be due to "induced-fit". The displacement between the N-atom of the K4 residue side chain in the two L27 structures is approximately 10 Å. The inset in Fig. 6 shows a zoom-out view of the relative positions of L27, tRNA and the P-loop. The N-terminal of L27 from the ribosome without tRNAs points to a different direction compared to the N-terminal of L27 interacting with the peptidyl tRNA. Combining with the structural information, our single molecule FRET study implies that the L27 rearranges its conformation in responding to tRNA binding and stabilizes the peptidyl tRNA.

3.1. Experimental section

3.1.1. Protein preparation

His-tagged proteins EF-G, EF-Tu and EF-Ts were expressed and purified using standard methods (Qiagen purification kit or Histrap FPLC column from GE healthcare). N-acetyl phenylalanine-tRNA was prepared essentially as described [29]. 5′-biotinylated 032mRNA was purchased from Dharmacon RNAi Technologies, Thermo Scientific. All the reagents were from Sigma unless otherwise stated.

3.1.2. L27 WT and mutants preparation

The *rpmA* gene encoding *E. coli* WT L27 was subcloned into the PET-20b plasmid from the PET-3b plasmid (a kind gift from Prof. J. Wower of Auburn University, Auburn, AL). The C-terminal

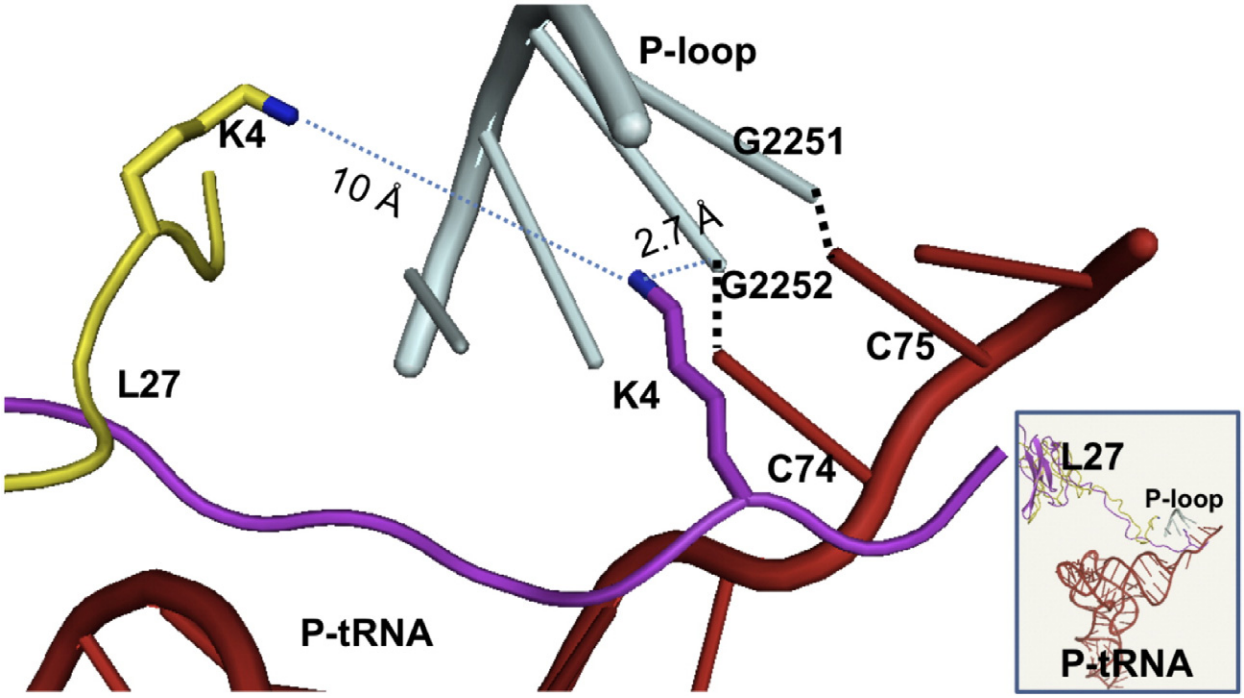

Fig. 6. The overlay structure of L27 from two different ribosome complexes from [15,28]. The inset shows the overall arrangements of the two L27 proteins (the magenta and yellow), the P-loop (light cyanine) and the P-site tRNA (red). In the ribosome bearing two complete tRNA substrates, the K4 residue of L27 (magenta) interacts with the P-loop (2.6 Å), which forms the cognate C-G base pair with C74 of P-site tRNA. In the ribosome bearing no tRNA substrate, the L27 (yellow) points to another direction without interacting with the P-site tRNA. The distance of the N atom on the K4 residue of the two structures is approximately 10 Å.

His-tagged L27 was expressed and purified according to standard procedures (Histrap FPLC column from GE healthcare). L27 mutant' plasmids were generated by QuickChange® Lightning site-directed mutagenesis from Stratagene. The protein sequences were confirmed by DNA sequencing as well as N-terminal protein sequencing with the Edman degradation method.

3.1.3. Ribosomes, Cy5-L27 and Cy3-tRNA^{Phe}

Ribosomes lacking L27 were isolated from *E. coli* strain IW312 as described [30], except that in the 10–40% sucrose gradient purification step the 70S is not dissociated. L27 WT and mutants were labeled at the unique C53 position with a Cy5-maleimide mono-reactive dye (GE Healthcare Life Sciences) dissolved in DMSO according to the provided protocol. Yeast tRNA^{Phe} (Sigma) was labeled at the 16/17 position with Cy3-hydrazide (GE healthcare) according to literature [24].

3.1.3.1. L27-labeled ribosomes [11,31]. The labeled L27 was incorporated into the ribosome 70S as described: the purified IW312 ribosomes (1 μM) were incubated with Cy5-labeled L27 (1.2 μM) in TAM_{10} buffer at 37 °C for 25 min. The solution was then layered on 1:1 volume ratio of 1.1 M sucrose and centrifuged at 35,000 rpm at 4 °C for 12 h using a Beckman SW 50.1 rotor. The pelleted ribosomes were resuspended in B2 buffer and stored in aliquot at −80 °C.

The incorporation efficiency of L27 into IW312 ribosome was 100%, whereas unspecific uptake of L27 into the MRE600 ribosome was 10%–20%. The correct position of L27 incorporation into the ribosome was confirmed by: (a) the complete recovery of IW312 ribosome activity after L27 incorporation; and (b) zero FRET signal from MRE600 ribosome with the nonspecific L27 uptake.

3.1.3.2. Ribosome complex formation [3,11]. The pre-translocation complex was made as described [31] and purified by sucrose cushion ultracentrifugation. Three mixtures were made. (1) The ribosome mixture contained 1 μM ribosomes, 4 mM GTP, 1.5 μM each of factors IF1, 2 and 3, 4 μM 032 mRNA which encoded MFK and six more amino acids and 4 μM formyl-Met-tRNA^{fMet} in TAM_{10} buffer; (2) the factor mixture contained 3 μM EF-Tu, 4 μM EF-Ts, 1 μM GTP, 1 mM phosphoenolpyruvate/ATP, and 0.006 mg/ml pyruvate kinase in TAM_{10} buffer; (3) the aminoacylation mixture contained 100 mM Tris (pH 7.5), 20 mM $MgAc_2$, 1 mM EDTA, 4 mM ATP, 7 mM BME, 1 mg/ml purified yeast total synthetase, 100 μM phenylalanine, and 2 A_{260}/ml Cy3-tRNA^{phe}. All three mixtures were incubated separately at 37 °C for 25 min, and then mixed at a ratio of 1:2:2 in the order of solutions (1), (2) and (3). The mixture was briefly incubated at 37 °C for another 2 min and layered on 1:1 volume ratio of 1.1 M sucrose and centrifuged overnight with a SW50.1 rotor at 35,000 rpm. The pre-translocation was then stored at −80 °C in aliquots.

The post-translocation complex was prepared by incubating the purified pre-complex (0.2 μM) with EF-G (1.0 μM), GTP (1 mM), phosphoenolpyruvate/ATP (1 mM) and pyruvate kinase (0.02 mg/ml) in an Eppendorf tube for 5 min at 37 °C. It was then fractioned and stored at −80 °C.

3.1.4. Puromycin assay

The puromycin assay is modified from the "SPARK" protocol [20]. The pre- and post-translocation complexes were prepared as described above, except that ^{3}H-labeled phenylalanine with high specific radioactivity was used instead of cold amino acid. Then, 60 μl of the ribosome complex with 12 pmol of ribosomes was incubated with 300 μM or 0 μM of puromycin at 37 °C for 15 min. Afterward, 120 μl of SPA beads (PerkinElmer, RPNQ0263) in TAM_{10} buffer (0.45 mg/ml) was added into the ribosome solution and incubated at room temperature for 2 h and then counted. The extent of the puromycin reaction was calculated by the difference of ^{3}H-counts between ribosomes with and without puromycin divided by the ^{3}H-counts of the ribosome solution without puromycin.

A second round of the puromycin assay was performed on the above ribosome solutions without puromycin. In these assays, the ribosome complexes were already tethered on the SPA beads

and then incubated with 300 μM puromycin at 37 °C for 15 min and then counted. The percentage of the puromycin reaction was calculated by the difference of ^{3}H-counts between the ribosome SPA solutions before and after puromycin addition divided by the ^{3}H-counts of the ribosome solution before puromycin addition.

3.1.5. Surface tethering of ribosomes

Glass cover-slips were cleaned and passivated with Biotin-PEG [32]. Streptavidin (0.5 mg/ml) was delivered to the surface before single-molecule acquisition. The ribosome complexes were then tethered to the surface via the streptavidin–biotinylated mRNA interaction.

3.1.6. TIRF measurements

The objective-based TIRF setup was built on a Nikon Eclipse Ti inverted microscope (Nikon Instruments, Lewisville, TX) with heavy modifications, as previously described [12]. Total internal reflection of a 6–12 mW, 532-nm laser beam through an objective (Nikon, Apo TIRF, 60×/1.49 oil) generated evanescent waves near the sample chamber surface to excite fluorophores bound to the surface (but not those in the bulk medium). The emitted FRET signals were split by a Dual View apparatus (Optical Insights Corp.), collected by an EMCCD camera (Photometrics, Cascade II: 512) and analyzed with an in-house algorithm based on ImageJ and Mathcad software. The emission maximum for the Cy3 and Cy5 dyes are at 570 nm and 670 nm, respectively.

The data were collected at 100-ms intervals. The final imaging buffer contained an oxygen scavenger cocktail with the following gradients: 3 mg/ml glucose, 100 μg/ml glucose oxidase, 48 μg/ml catalase and 2 mM trolox [25,28].

Acknowledgments

This work is supported by the Welch Foundation (E-1721). We are thankful for the kind gifts of the IW312 ribosome glycerol stock from Prof. Robert A. Zimmermann (University of Massachusetts at Amherst) and plasmids from Profs. Yale E. Goldman (University of Pennsylvania), Barry S. Cooperman (University of Pennsylvania), Rachel Green (the Johns Hopkins University) and Jacek Wower (Auburn University).

Appendix A. Supplementary data

Supplementary data to this article can be found online at http://dx.doi.org/10.1016/j.bpc.2012.04.003.

References

[1] J. Frank, R.K. Agrawal, A ratchet-like inter-subunit reorganization of the ribosome during translocation, Nature 406 (2000) 318–322.
[2] D. Moazed, H.F. Noller, Intermediate states in the movement of transfer RNA in the ribosome, Nature 342 (1989) 142–148.
[3] C.T. Ly, M.E. Altuntop, Y. Wang, Single-molecule study of viomycin's inhibition mechanism on ribosome translocation, Biochemistry 49 (2010) 9732–9738.
[4] J.B. Munro, R.B. Altman, C.S. Tung, K.Y. Sanbonmatsu, S.C. Blanchard, A fast dynamic mode of the EF-G-bound ribosome, The EMBO Journal 29 (2010) 770–781.
[5] J. Fei, P. Kosuri, D.D. MacDougall, R.L. Gonzalez Jr., Coupling of ribosomal L1 stalk and tRNA dynamics during translation elongation, Molecular Cell 30 (2008) 348–359.
[6] D.N. Ermolenko, P.C. Spiegel, Z.K. Majumdar, R.P. Hickerson, R.M. Clegg, H.F. Noller, The antibiotic viomycin traps the ribosome in an intermediate state of translocation, Nature Structural & Molecular Biology 14 (2007) 493–497.
[7] X. Agirrezabala, J. Lei, J.L. Brunelle, R.F. Ortiz-Meoz, R. Green, J. Frank, Visualization of the hybrid state of tRNA binding promoted by spontaneous ratcheting of the ribosome, Molecular Cell 32 (2008) 190–197.
[8] A. Savelsbergh, V.I. Katunin, D. Mohr, F. Peske, M.V. Rodnina, W. Wintermeyer, An elongation factor G-induced ribosome rearrangement precedes tRNA–mRNA translocation, Molecular Cell 11 (2003) 1517–1523.
[9] M. Valle, A. Zavialov, J. Sengupta, U. Rawat, M. Ehrenberg, J. Frank, Locking and unlocking of ribosomal motions, Cell 114 (2003) 123–134.
[10] P.V. Cornish, D.N. Ermolenko, H.F. Noller, T. Ha, Spontaneous intersubunit rotation in single ribosomes, Molecular Cell 30 (2008) 578–588.
[11] M.E. Altuntop, C.T. Ly, Y. Wang, Single-molecule study of ribosome hierarchic dynamics at the peptidyl transferase center, Biophysical Journal 99 (2010) 3002–3009.
[12] C.E. Aitken, J.D. Puglisi, Following the intersubunit conformation of the ribosome during translation in real time, Nature Structural & Molecular Biology 17 (2010) 793–800.
[13] D. Moazed, H.F. Noller, Interaction of tRNA with 23S rRNA in the ribosomal A, P, and E sites, Cell 57 (1989) 585–597.
[14] D.N. Ermolenko, Z.K. Majumdar, R.P. Hickerson, P.C. Spiegel, R.M. Clegg, H.F. Noller, Observation of intersubunit movement of the ribosome in solution using FRET, Journal of Molecular Biology 370 (2007) 530–540.
[15] R.M. Voorhees, A. Weixlbaumer, D. Loakes, A.C. Kelley, V. Ramakrishnan, Insights into substrate stabilization from snapshots of the peptidyl transferase center of the intact 70S ribosome, Nature Structural & Molecular Biology 16 (2009) 528–533.
[16] B.A. Maguire, A.D. Beniaminov, H. Ramu, A.S. Mankin, R.A. Zimmermann, A protein component at the heart of an RNA machine: the importance of protein L27 for the function of the bacterial ribosome, Molecular Cell 20 (2005) 427–435.
[17] Xiao, M. & Wang, Y., Ribosome subpopulation analysis reveals the possible role of L27 at the peptidyl transfer center, FEBS J. submitted for publication.
[18] C. Flinta, B. Persson, H. Jornvall, G. von Heijne, Sequence determinants of cytosolic N-terminal protein processing, European Journal of Biochemistry 154 (1986) 193–196.
[19] I.K. Wower, J. Wower, R.A. Zimmermann, Ribosomal protein L27 participates in both 50S subunit assembly and the peptidyl transferase reaction, The Journal of Biological Chemistry 273 (1998) 19847–19852.
[20] A.S. Mankin, N. Polacek, SPARK: a new peptidyl transferase activity assay, Methods in Molecular Medicine 142 (2008) 107–116.
[21] D. Pan, S.V. Kirillov, B.S. Cooperman, Kinetically competent intermediates in the translocation step of protein synthesis, Molecular Cell 25 (2007) 519–529.
[22] F. Peske, A. Savelsbergh, V.I. Katunin, M.V. Rodnina, W. Wintermeyer, Conformational changes of the small ribosomal subunit during elongation factor G-dependent tRNA–mRNA translocation, Journal of Molecular Biology 343 (2004) 1183–1194.
[23] A.V. Zavialov, M. Ehrenberg, Peptidyl-tRNA regulates the GTPase activity of translation factors, Cell 114 (2003) 113–122.
[24] D. Pan, H. Qin, B.S. Cooperman, Synthesis and functional activity of tRNAs labeled with fluorescent hydrazides in the D-loop, RNA 15 (2009) 346–354.
[25] D.N. Ermolenko, H.F. Noller, mRNA translocation occurs during the second step of ribosomal intersubunit rotation, Nature Structural & Molecular Biology 18 (2011) 457–462.
[26] S. Dorner, J.L. Brunelle, D. Sharma, R. Green, The hybrid state of tRNA binding is an authentic translation elongation intermediate, Nature Structural & Molecular Biology 13 (2006) 234–241.
[27] R.R. Samaha, R. Green, H.F. Noller, A base pair between tRNA and 23S rRNA in the peptidyl transferase centre of the ribosome, Nature 377 (1995) 309–314.
[28] B.S. Schuwirth, M.A. Borovinskaya, C.W. Hau, W. Zhang, A. Vila-Sanjurjo, J.M. Holton, J.H. Cate, Structures of the bacterial ribosome at 3.5 A resolution, Science 310 (2005) 827–834.
[29] J.M. Robertson, W. Wintermeyer, Effect of translocation on topology and conformation of anticodon and D loops of tRNAPhe, Journal of Molecular Biology 151 (1981) 57–79.
[30] D. Moazed, B.J. Van Stolk, S. Douthwaite, H.F. Noller, Interconversion of active and inactive 30S ribosomal subunits is accompanied by a conformational change in the decoding region of 16S rRNA, Journal of Molecular Biology 191 (1986) 483–493.
[31] Y. Wang, H. Qin, R.D. Kudaravalli, S.V. Kirillov, G.T. Dempsey, D. Pan, B.S. Cooperman, Y.E. Goldman, Single-molecule structural dynamics of EF-G–ribosome interaction during translocation, Biochemistry 46 (2007) 10767–10775.
[32] R. Roy, S. Hohng, T. Ha, A practical guide to single-molecule FRET, Nature Methods 5 (2008) 507–516.